metals

Article

Precipitation Behavior of ω Phase and ω→α Transformation in Near β Ti-5Al-5Mo-5V-1Cr-1Fe Alloy during Aging Process

Yi Guo [1], Shaohong Wei [2,3], Sheng Yang [4], Yubin Ke [2,3], Xiaoyong Zhang [1,*] and Kechao Zhou [1]

[1] State Key Laboratory of Powder Metallurgy, Central South University, Lu Mountain South Road, Changsha 410083, China; guo-yi@csu.edu.cn (Y.G.); zhoukechao@csu.edu.cn (K.Z.)
[2] Spallation Neutron Source Science Center (SNSC), Dongguan 523808, China; weish@ihep.ac.cn (S.W.); keyb@ihep.ac.cn (Y.K.)
[3] Dongguan Research Department, Institute of High Energy Physics (IHEP), Chinese Academy of Sciences (CAS), Dongguan 523808, China
[4] Hunan Goldsky Titanium Industry Technology Co., Ltd., No. 97 Qianming Road, Deshan Town, Changde ECO-TECH Development Zone, Changde 415001, China; 13874850716@163.com
[*] Correspondence: zhangxiaoyong@csu.edu.cn

Abstract: In this work, the precipitation behavior of the ω phase and ω→α transformation in Ti-5Al-5Mo-5V-1Cr-1Fe (Ti-55511) alloy was investigated during isothermal aging at 450 °C. The results show that the α precipitates increase with the increasing of aging time, resulting from the β→α and ω→α transformations. The ω→→α transformation involves the formation and evolution of the isothermal ω phase. The formation of the isothermal ω phase occurs after 30 min and ends at 120 min, which is caused by the embryonic ω phase to isothermal ω phase transformation. Small angle neutron scattering (SANS) results indicates that the evolution of the isothermal ω phase goes through the increasing average size and aspect ratio from 24.7 to 47.0 nm and from 2.1 to 2.7 respectively, and the morphology evolution of the ω particle from ellipsoid to spindle-like. Moreover, the isothermal ω phase assists the α phase to nucleate at the ω/β interface, which involves the changes in elemental composition. The α phase is enriched in Al. Compared to the α phase, the element of Mo, V and Cr in the isothermal ω phase is lower. The Fe element is uniformly distributed in the isothermal ω phase and β matrix but lean in the α phase.

Keywords: precipitation behavior; Ti-55511; aging process; isothermal ω phase; SANS

1. Introduction

Near β-titanium alloys have received great attention as the main materials for aerospace application in section forgings and fasteners because of their outstanding properties, including ultra-high specific strength, excellent fracture toughness and yield strength [1–5]. For example, Ti-10V-2Fe-3Al (Ti-1023) and Ti-5Al-5Mo-5V-3Cr (Ti-5553) alloy have been widely used in the landing gear of Airbus and Boeing passenger aircraft, respectively [6,7]. In addition, Ti–5Al–5Mo–5V–1Cr–1Fe (Ti-55511) near β titanium alloy (also called TC18 alloy) has good comprehensive properties, including the light weight, high strength and good fatigue performance. It has excellent plasticity and toughness at room temperature, and its tensile strength can reach more than 1150 MPa [8–10].

The excellent performances of near β-titanium alloys are mainly ascribed to its improved internal microstructures. Precipitation of the small dispersed α phase in the β matrix by appropriate processing methods and heat treatment is an effective method to achieve improved microstructures to obtain ultra-high performances [11–13]. However, the necessary nucleation sites for α precipitating are usually absent in near β-titanium alloys [14]. In addition, near β-titanium alloy has a high content of β stabilizers, such as Mo, V and others. Due to the low diffusion rate, the diffusion distance of Mo is short during rapid cooling or low temperature aging, which means that the β matrix can be

retained [15]. Generally, when quenched from high temperature (above the β transus), the β matrix would precipitate the athermal ω phase as a transient phase [16]. After isothermal aging treatment at a lower temperature (<500 °C), athermal β matrix would convert into the isothermal ω phase with a hexagonal structure [17,18]. In general, the ω phase is considered as an effective nucleation assistant to promote the dispersed precipitation of the α phase [19]. However, not all types of ω phases can be used as α nucleation assistant. It was reported that the athermal ω phase had not shown the ability to assist the nucleation of the α phase [20,21]. The embryonic ω phase (also called the incommensurate ω phase, and is considered as the precursor of isothermal ω phase) has also no direct effect on the formation of α phase [22]. Whereas, the commensurate isothermal ω phase promotes the nucleation of the α phase zealously [23].

The dispersed precipitation of isothermal ω phase has a positive effect on precipitation and refinement of intragranular α phase, which provides an idea for improving the properties of alloys. For this purpose, the nature of the ω→α transformation has been discussed for many years. For now, two transformation mechanisms are widely recognized. The first is that α phase nucleates near the ω/β interface, which is attributed to the formation of Al-rich region during formation of ω phase [24]. The second mechanism demonstrates that ω→α transformation is a mixed-mode including reconstruction of ω/β interface and diffusion of Al element [12,23]. To further elaborate the mechanism of ω-assisted α nucleation, the impact of ω/β interface on α phase nucleation in the metastable β alloy was revealed, which was related to the size and morphology of isothermal ω phase [25,26]. In other words, the size and morphology of ω phase has a certain effect on the nucleation of α phase. In general, the isothermal ω is shown as ellipsoidal shape in low β-ω misfit or cubic shape in high β-ω misfit [19,27]. The mechanism of the ω phase with an ellipsoidal or cubic shape on the α nucleation has been proposed [28,29]. However, the research on the statistical particles size measurement of the ω phase during the early stage of the aging process is still limited. The size of the ω particle was generally measured by multiple inverse Fourier filtered transform (IFFT) images or dark field TEM images [23,30,31]. Nevertheless, the amount of ω particles measured by this method is usually low, and the data may not be representative since the distribution of ω phase may not uniform in some areas. Therefore, conducting a large number of statistical sizes of ω particles is needed.

In present study, the precipitation behavior of the ω phase and ω→α transformation in near β Ti-55511 alloy was studied during the aging process, including particle morphology, size, chemical distribution and formation of α assisted by ω phase. The phase composition was analyzed by X-ray diffraction (XRD) during the aging process. Transmission electron microscopy (TEM) and high-angle annular dark field scanning transmission electron microscopy (HAADF-STEM) tests were conducted to observe and confirm the nano-scale particles precipitated during aging process. In addition, the small angle neutron scattering (SANS) technique was applied to analyze the morphology and statistical size of the dispersed nano-scale precipitates.

2. Materials and Methods

Ti-55511 ingot for this work was provided by Hunan Goldsky Titanium Company (Changde, China). The raw ingot was prepared by vacuum arc-melting firstly, and forged to the bars with a diameter of 500 mm subsequently. The samples were carried out at 920 °C (above 875 °C transus) for 2 h firstly, followed by water quenching. Subsequently, a series of aging treatments were performed on the β-quenched specimens. Generally, the ω phase precipitates during isothermal aging at low temperature (below 500 °C) [18]. In order to better obtain the ω phase to study its precipitation behavior, aging temperature of 450 °C was designed. Aging times of 15, 30, 60 and 120 min were chosen. All aged samples were water-quenched to retain their microstructures.

The aged specimens were tested for via XRD, SANS and TEM. The XRD test was examined using the instrument (Lausanne, Switzerland) made in The Brock Company in Switzerland. The instrument uses Cu-Kα radiation with 40 KV voltage and 40 mA current.

Specimens for TEM and HAADF-STEM tests were prepared by mechanical thinning firstly, and then electropolished using twin-jet thinning technology with the condition parameter of $-25\,^{\circ}C$ and 30 V, in which the solution was composed of $CH_3(CH_2)_3OH$ (35%), $HClO_4$ (5%) and CH_3OH. TEM images were observed using Titan G2 60–300 high resolution spherical aberration correction TEM (FEI, Hillsboro, OR, USA) at an accelerating voltage of 300 KV. Microstructures of HAADF-STEM specimens were examined using the Talos F200X instrument (FEI, Brno, Czech) at 200 KV.

In this study, the SANS measurement was conducted at China Spallation Neutron Source (CSNS, Dongguan, China) [32]. During the experiment, the sample to detector distance was set to 4 m and the diameter of sample aperture was 6 mm. The selected incident neutrons wavelength is 1–10 Å, which can cover a wide Q range from 0.005 Å^{-1} to 0.60 Å^{-1}. To obtain high quality data, we collected approximate 90 min scattering information for each sample. The scattering data were set to absolute unit after normalization, background subtraction and correction with transmission and standard sample calibration.

3. Results and Discussion

3.1. Phase Transformation during Aging Process

Figure 1 shows the XRD patterns of different aged samples at 450 $^{\circ}$C. An extremely weak peak appears in XRD pattern for solution treatment (ST) samples. It's supposed to be α'' phase, produced by non-diffusion shear of β matrix [33]. The α phase peak at 35.2° (labelled (010)α) appears at 15 min. It is evident that, α phase precipitates at early aging time. With the increasing aging time at 450 $^{\circ}$C, the peak intensity of α phase arise clearly, which indicates the enhancement of α precipitates. Compared with the intensity of the other α peaks, the higher relative intensity of the (010)α peak resulted from the preferential precipitation of the α phase during the aging process, which was in accordance with the previously reported Burgers relationships between β and α, ω and α: $\{110\}_\beta//\{0001\}_\alpha$, $(11\bar{2}0)_\omega//(0001)_\alpha$ [34,35]. This may be the result of $\beta\rightarrow\alpha$ and/or $\omega\rightarrow\alpha$ transformations.
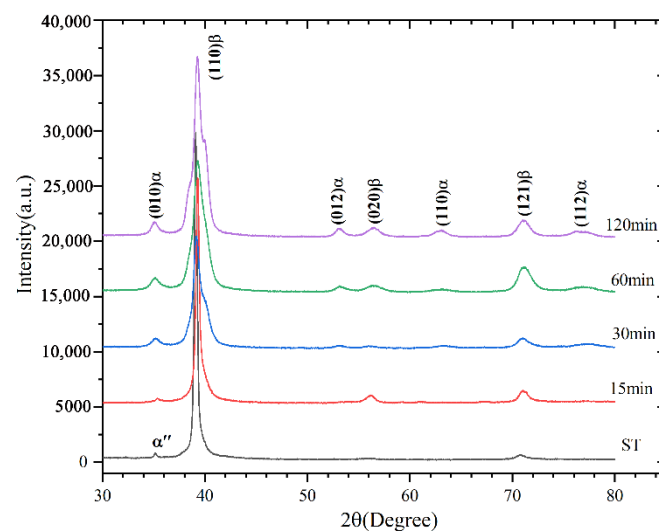
Figure 1. XRD patterns of samples solution treatment (ST) at 920 $^{\circ}$C/2 h and aged at 450 $^{\circ}$C for different times.

However, the peaks of the ω phase are not observed in the XRD patterns. The $\omega\rightarrow\alpha$ process still needs further direct evidences. For this purpose, HAADF-STEM analysis was performed, as shown in Figure 2. From Figure 2a, a large amount of short rod-shaped α precipitates after aging for 15 min. The triangle-like distribution of some α precipitates suggests that these α phases are directly precipitated from β matrix and satisfy the Burgers relationship. Meanwhile, the long needle-shaped α phase near the ellipsoidal ω phase can also observed in Figure 2b. It provides evidence that the α is formed by the ellipsoidal ω phase and β matrix together at 60 min. Only the isothermal ω would directly participate

in the formation of α [23]. Therefore, it can be seen that the isothermal ω precipitates and participates in the formation of α at 60 min. Combined with the XRD results, the formation of α is the result of the β→α and ω→α transformations. In the early stage of aging, the β→α transformation occurs. With the aging time increases, the precipitated the ω phase participates in the precipitation of α phase. The aging time required for the isothermal ω phase to start to assist the precipitation of α phase was 4–8 h at a low aging temperature [23,36]. In this work, the aging temperature of 450 °C significantly accelerates the formation of α phase. This may be caused by two reasons. On the one hand, the high aging temperature can provide the sufficient driving force for β→α transformation. On the other hand, a high elemental diffusion rate given by a high aging temperature can promote the formation of isothermal ω phase which assists the precipitates of α phase.
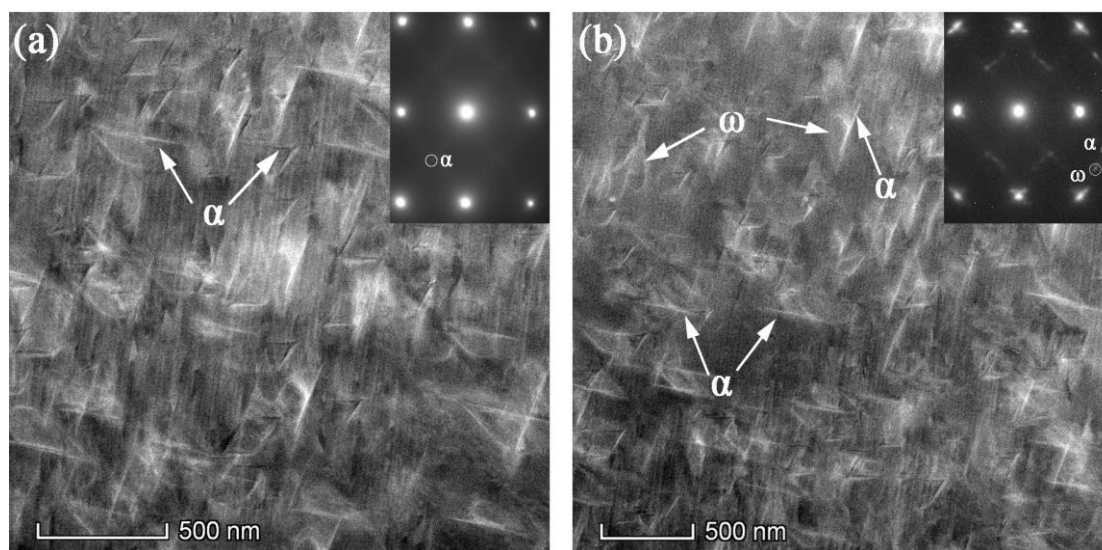
Figure 2. High-angle annular dark field scanning transmission electron microscopy (HAADF-STEM) images showing the microstructure of Ti-55511 aged for (**a**) 15 min at 450 °C and (**b**) 60 min at 450 °C.

3.2. Formation of Isothermal ω Phase

Although the isothermal ω→α transformation is confirmed at the later aging process (Figure 2), the question arises of how the isothermal ω phase assisted in the formation of α phase was formed. For this, the selected-area electron diffraction (SAED) images observed along the $[110]_\beta$ zone axis for different aging times at 450 °C is shown in Figure 3. After aging for 15 min, the existence of diffuse scattering streaking is observed. The reflections at 1/3 and 2/3 <112>β appear as lines. The diffuse scattering streaking is attributed to the embryonic ω phase [7,37]. After increasing aging time to 30 min (Figure 3b), the diffuse scattering streaking begins to weaken, and the spots at 1/3 and 2/3 <112>β appear. This provides the evidence showing that the remaining embryonic ω phase further transforms to the isothermal ω phase. After aging for 60 min (Figure 3c), the diffuse scattering streaking disappears and distinct spots appear, indicating that the embryonic ω phase transforms into the isothermal ω phase completely and the amount of isothermal ω precipitates increase. The spots in Figure 3c, d clearly show that the relationships between ω, α and β satisfy the following: $(111)_\beta//(0001)_\omega//(11\bar{2}0)_\alpha$ [38]. In other words, the formation of isothermal ω is a continuous process involving the transformation of embryonic ω phase to isothermal ω phase. The transformation process starts beginning with 15 min and ends at 120 min.

In order to visually observe the information of isothermal ω phase, dark field images were performed to assist SAED analysis. Figure 4a shows sparsely close ellipsoidal ω particles, which is typical for the near β titanium alloys, such as in Ti-5Al-5Mo-5V and Ti-7Mo-3Al-3Cr-3Nb [16,39]. From the analysis of Figure 3b–d, it suggests that the em-

bryonic ω phase and isothermal ω phase already coexist after 30 min of aging. With the increasing aging time, the formation step-by-step of isothermal ω phase is obvious. Moreover, the ω phase distribution becomes denser and the size is larger, reaching the maximum after aging for 120 min (Figure 4d). It is clear that the formation of isothermal ω involves the size change of ω particles. However, the distribution of ω particles is not uniform. There are many smaller ω particles distributing around the larger ω phase, and the unique phenomenon of small ω agglomeration appear in some areas. Therefore, the SANS technique is used in this work, which can probe the dispersed ω phase in the entire neutron penetration volume of the bulk sample, which usually can provide a reliable statistical information of the nano-scale inhomogeneity within ~0.1 cm^3.
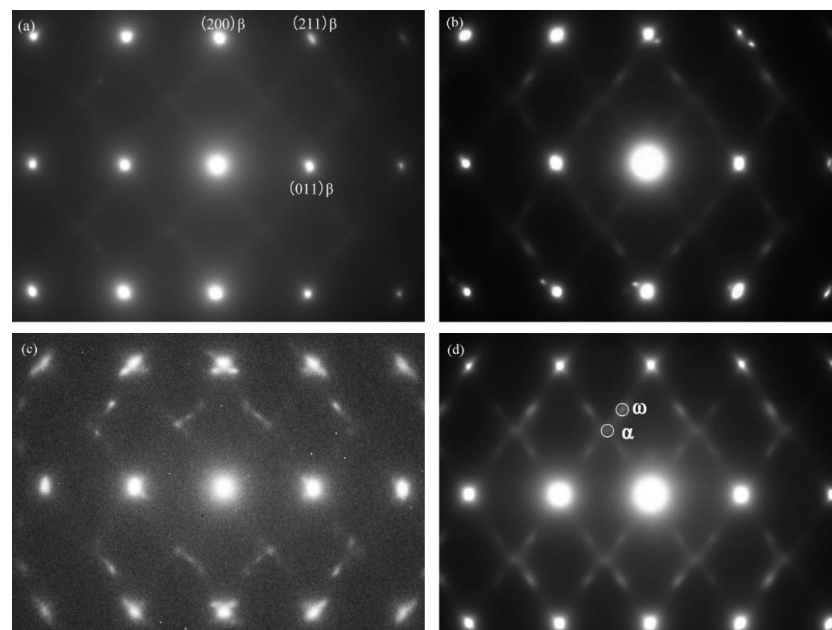
Figure 3. Selected area diffraction patterns of Ti-55511 after aging for (**a**) 15 min, (**b**) 30 min, (**c**) 60 min, (**d**) 120 min taken from the $[110]_\beta$ zone axis.
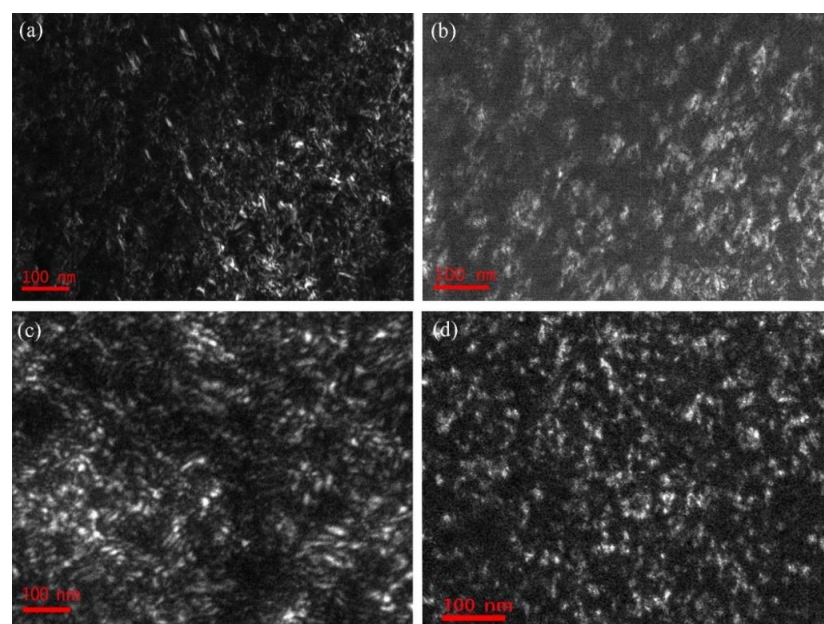
Figure 4. Dark field TEM images of Ti-55511 samples aged for (**a**) 15 min, (**b**) 30 min, (**c**) 60 min, (**d**) 120 min taken from 1/3 <112> reflection spot.

3.3. Evolution of Isothermal ω Phase

Figure 5 shows the result of the SANS test conducted at room temperature with different aged samples. By using an incident neutron wavelength of 1~10 Å, the scattering intensity as a function of scattering vector Q was collected in the range from 0.005 Å^{-1} to 0.6 Å^{-1}. As shown in Figure 5, the scattering intensity arises gradually as the aging time increases and changes sharply after aging for 30 min. With aging time increasing, the embryonic ω transforms to isothermal ω and causes the growth of scattering intensity, which is proportional to the volume fraction of nano-scale α precipitates. After aging for 60 min, the intensity difference was expanded due to the large number of nanoparticles α precipitates assisted by isothermal ω phase.
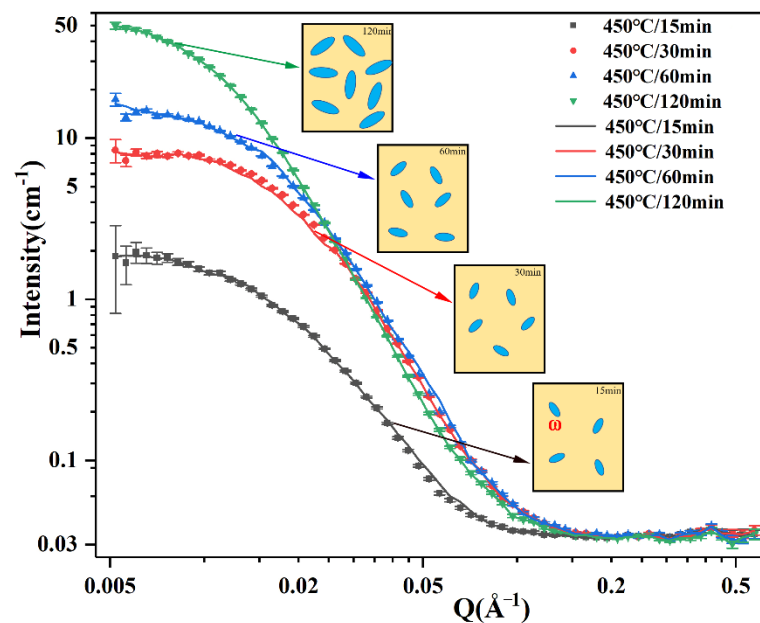
Figure 5. The SANS curves measured at room temperature of the aged Ti-55511 samples. The figure is plotted on a log-log scale. A schematic diagram of the evolution of ω particles is also shown.

To deduce the ω phase evolution, an elliptical particle model is employed to fit the observed SANS data by using the Sasview software [40]. According to this model the scattering intensity can be described by using the following function [41]:

$$I(q) = \frac{scale}{V}F^2(Q) + background, \tag{1}$$

where

$$F(q) = \Delta\rho V \frac{3(\sin qr - qr\cos qr)}{(qr)^3}, \tag{2}$$

for

$$r = [R_e^2 + R_p^2]^{1/2}, \tag{3}$$

where, scale is source intensity, $V = (4/3)\pi R_p R_e^2$ is the volume of one ellipsoid particle. R_p and R_e are the polar radius and the equatorial radius of the ellipsoid particle model, respectively. $\Delta\rho$ (contrast) is the difference of the scattering length density between the scatter particle and matrix. The background is used to avoid the influence of incoherent scattering. In the fitting process, the hard sphere structure factor is used as the structure factor which is defined as 1 due to the low volume fraction of precipitated phase. Equatorial radius and polar radius of the ω particles are obtained after fitting. The length (twice the equatorial radius) and width (twice the polar radius) of ω phase are obtained from the fitting parameters and plotted as a function of aging time in Figure 6. As it is shown,

average size of the ω particle reaches a length of 24.7 nm and a width of 11.8 nm at 15 min. Subsequently, the size of ω particle changes slightly at 30 min, but grows significantly after 60 min. After aging for 120 min, the ω precipitates grow to a maximum with length of 47.0 nm and width of 16.8 nm. Furthermore, the ratio of the equatorial radius axis and polar radius is also shown in Figure 6, which demonstrates a noteworthy change. According to the results (Figures 4 and 6), the schematic diagram of the ω particles is shown in Figure 5. With increasing aging time, the changes that occur in the ω particles are clearly displayed. The aspect ratio increases from 2.1 to 2.7, which suggests the transition from ellipsoidal-shaped embryonic ω phase to spindle-shaped isothermal ω phase.
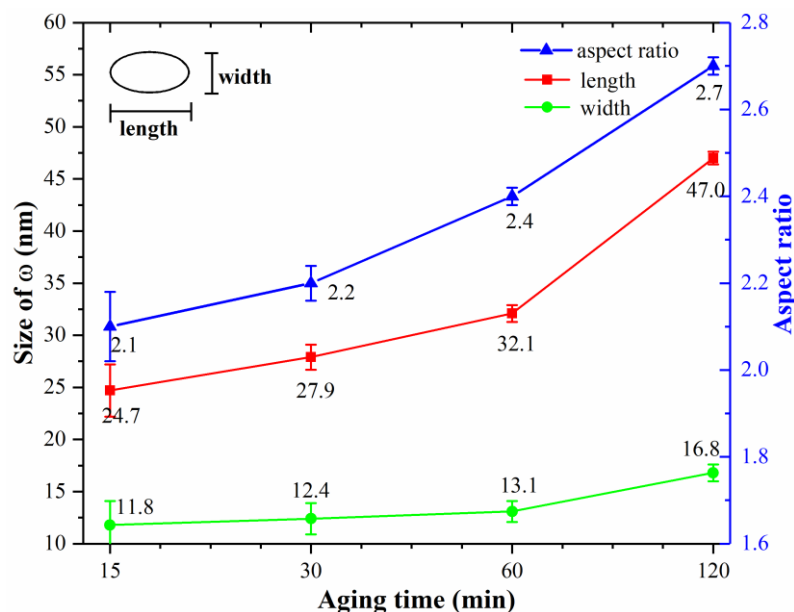
Figure 6. The average size parameters of ω particles obtained by small angle neutron scattering SANS) data. The size parameters are obtained by doubling the value of equatorial radius and polar radius to intuitively reflect the size of ω particles. The aspect ratios of ω particles are also shown.

Generally speaking, the aging process promotes the continuous increase of the size of ω phase, and the aspect ratio increases significantly after aging for 60 min. Combining the previous results (Figures 3 and 4), it is that the evolution of ω phase involves changes in the size and morphology. The embryonic ω phase to isothermal ω phase transformation causes an increasing average size. The size evolution of the ω particles involves a noteworthy change in the aspect ratio, which may result from the structural difference between embryonic ω phase and isothermal ω phase. The structural difference between embryonic ω and isothermal ω is attribute to constrain by coherent elastic strain [23]. Because of this elastic strain, the isothermal ω precipitates was observed to be slightly elongated along its length axis, compared to the embryonic ω precipitates. In the previous analysis (Figures 2 and 3), it has been known that the embryonic ω phase and isothermal ω phase coexist at 30 min of aging. In the SANS results, the sizes of the embryonic ω and isothermal ω are counted indistinguishably at 15 min and 30 min aging, and the average size is obtained in the fitting. The ratio of ω changes proves that the proportion of embryonic ω has little change at 15 and 30 min. After 60 min, the embryonic ω phase transforms into the isothermal ω phase completely, which causes the aspect ratio significantly different than before. In summary, the evolution of ω particles goes through the increase in size and particle density, and the transformation of the morphology from ellipsoid to like spindle. Among them, the conversion of embryonic ω phase → isothermal ω phase causes the aspect ratio change.

3.4. ω Assisted α Nucleation

The direct observation of isothermal ω assisting α formation is shown in Figure 2b. For more detailed information, the HRTEM image of sample aged at 450 °C/120 min recorded along the $[113]_\beta$ axis is shown in Figure 7a, and the FFT results at three regions corresponding to β, α and ω phase are shown in Figure 7b–d, respectively. The result proves that the α nucleates at surface of isothermal ω phase and grows into the β matrix. This is similar with what was observed in Ref. [23]. Ledges are visible at β/ω and ω/α interface. The β/ω interface plays an effective role in formation of α phase. The reasons for the existence of ledges at β/ω interface is that ledges lower the interfacial energy and relax the coherency strain energy [42]. The α phase grows near isothermal ω phase and satisfies the reported orientation relationship: $(10\bar{1}0)_\alpha//(1\bar{1}00)_\omega//(211)_\beta$ [43].
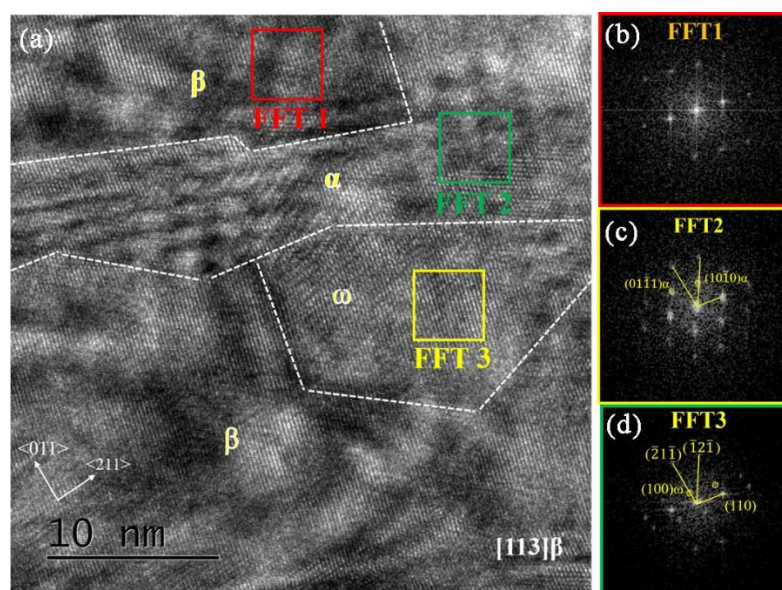
Figure 7. (**a**) Aberration corrected HRTEM image of the sample aged for 120 min at 450 °C taken along $[113]_\beta$ zone axis; (**b**) Fourier filtered transform (FFT) image of area 1; (**c**) FFT image of area 2; (**d**) FFT image of area 3.

In order to investigate the chemical distribution of the ω phase and α phase, HAADF-STEM mapping images of the sample treated at 450 °C/120 min were shown in Figure 8. The α grows in the side of isothermal ω is observed. Due to the long aging time (120 min), the α grows intensively and part of the α has been slatted. The growth of α is constrained after touching other α, so that the growth of α presents a dendritic cross growth, as shown in Figure 8a. Figure 8c–g shows the distribution of different elements in ω phase and α phase. It can be observed from the mapping images that Mo, V and Cr are almost not enrich in α phase, while Al is enriched in α phase with a larger content. For the ω phase, the content of Mo, V, and Cr is lower than that of the β matrix. The Fe element is relatively low in the Ti-55511 alloy, and it is less distributed in α phase, but is evenly distributed in β matrix and ω phase. The element distribution differences are clear between the ω and α phase. The main reason is that these elements play different roles in the formation of the different phases. Mo, V and Cr are β-stabilizing elements, and Al is α-stabilizing element. When isothermal ω is formed, ω discharges Al which is a α-stabilizer, and the content of Mo, V, Cr discharges to the β matrix is also reduced. When the isothermal ω phase assists the formation of α phase, the Al element accumulates in α as stable component.
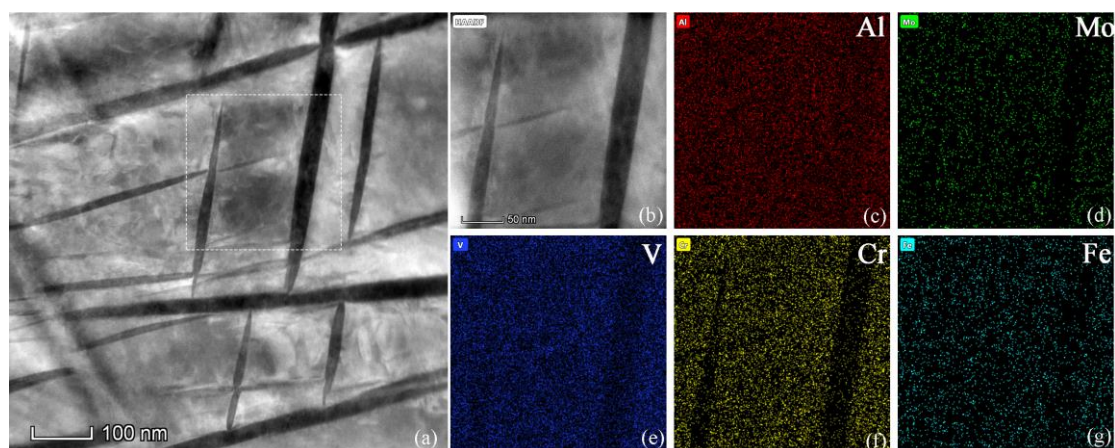
Figure 8. (**a**) HAADF-STEM image of the Ti-55511 sample aged for 120 min at 450 °C; (**b**) the image large magnification image of corresponding area in (a); (**c**–**g**) the element distribution mapping images of Al, Mo, V, Cr and Fe, respectively.

4. Conclusions

The precipitation behavior of the ω phase and ω→α transformation in the early aging process of Ti-55511 alloy was investigated. For this purpose, XRD, TEM and SANS tests were used. The formation of the α phase, the formation and evolution of the ω phase during the aging process and the formation of the α assisted by ω phase have been studied carefully. The specific conclusions obtained in this work are as follows:

1. The increased α precipitates are the result of the joint action of β→α and ω→α transformation processes. When the aging condition is 450 °C/30 min, the isothermal ω phase has coexisted with the embryonic ω phase. This may be due to the aging temperature of 450 °C accelerating the element diffusion process, which can promote the transformation process from the embryonic ω phase to the isothermal ω phase.

2. The embryonic ω phase precipitates at 15 min is not obvious. As the aging time continues to increase, the embryonic ω phase precipitates and transforms to isothermal ω phase after 30 min of aging. The transformation process completes after 120 min. The evolution of the isothermal ω phase goes through the increasing average size and aspect ratio from 24.7 to 47.0 nm and from 2.1 to 2.7 respectively, and the change of the ω particle morphology goes from ellipsoid to spindle-like with the increasing aging time.

3. The α phase nucleates at the ω/β interface and satisfy the orientation relationship: $(10\bar{1}0)_\alpha//(1\bar{1}00)_\omega//(211)_\beta$. The element of Mo, V and Cr in the isothermal ω phase is low. Additionally, Al, as an α stabilizing element, is enriched in the α phase. The Fe elements are evenly distributed in the isothermal ω phase and β matrix but lean in the α phase.

Conflicts of Interest: The authors declare no conflict of interest.

References

1. Banerjee, D.; Williams, J. Perspectives on titanium science and technology. *Acta Mater.* **2013**, *61*, 844–879. [CrossRef]
2. Boyer, R.R.; Briggs, R.D. The use of beta titanium alloys in the aerospace industry. *J. Mater. Eng. Perform* **2005**, *14*, 681–685. [CrossRef]
3. Ankem, S.; Greene, C.A. Recent developments in microstructure/property relationships of beta titanium alloys. *Mater. Sci. Eng. A* **1999**, *263*, 127–131. [CrossRef]
4. Okulov, I.V.; Wendrock, H.; Volegov, A.S.; Attar, H.; Kühn, U.; Skrotzki, W.; Eckert, J. High strength beta titanium alloys: New design approach. *Mater. Sci. Eng. A.* **2015**, *628*, 297–302. [CrossRef]
5. Okulov, I.V.; Bönisch, M.; Volegov, A.S.; Shahabi, H.S.; Wendrock, H.; Gemming, T.; Eckert, J. Micro-to-nano-scale deformation mechanism of a Ti-based dendritic-ultrafine eutectic alloy exhibiting large tensile ductility. *Mater. Sci. Eng. A.* **2017**, *682*, 673–678. [CrossRef]
6. Franco, L.A.L.; Lourenco, N.J.; Graca, M.L.A.; Silva, O.M.M.; De Campos, P.P.; Von Dollinger, C.F.A. Fatigue fracture of a nose landing gear in a military transport aircraft. *Eng. Fail. Anal.* **2006**, *13*, 474–479. [CrossRef]
7. Warchomicka, F.; Poletti, C.; Stockinger, M. Study of the hot deformation behavior in Ti-5Al-5Mo-5V-3Cr. *Mater. Sci. Eng. A* **2008**, *490*, 369–377.
8. Li, C.; Zhang, X.Y.; Zhou, K.C.; Peng, C.Q. Relationship between lamellar α evolution and flow behavior during isothermal deformation of Ti–5Al–5Mo–5V–1Cr–1Fe near β titanium alloy. *Mater. Sci. Eng. A* **2012**, *558*, 668–674. [CrossRef]
9. Tsybanev, G.V.; Ageev, M.A.; Titarenko, R.V. Analysis of the specific features of loading of the elements of landing gears of aircrafts aimed at the evaluation of the load-bearing capacity of the structure. *Strength Mater.* **2008**, *40*, 458–462. [CrossRef]
10. Lan, C.; Wu, Y.; Guo, L.; Chen, H.; Chen, F. Microstructure texture evolution and mechanical properties of cold rolled Ti-32.5Nb-6.8Zr-2.7Sn biomedical beta titanium alloy. *J. Mater. Sci. Technol.* **2018**, *34*, 788–792. [CrossRef]
11. Cotton, J.D.; Briggs, R.D.; Boyer, R.R.; Tamirisakandala, S.; Russo, P.; Shchetnikov, N.; Fanning, J.C. State of the art in beta titanium alloys for airframe applications. *JOM* **2015**, *67*, 1281–1303. [CrossRef]
12. Haghighi, S.E.; Attar, H.; Okulov, I.V.; Dargusch, M.S.; Kent, D. Microstructural evolution and mechanical properties of bulk and porous low-cost Ti-Mo-Fe alloys produced by powder metallurgy. *J. Alloys Compd.* **2021**, *853*, 156768. [CrossRef]
13. Chen, W.; Wang, H.D.; Lin, Y.C.; Zhang, X.Y.; Chen, C.; Zhou, Y.P.L.K.C. The dynamic responses of lamellar and equiaxed near β-Ti alloys subjected to multi-pass cross rolling. *J. Mater. Sci. Technol.* **2020**, *43*, 220–229. [CrossRef]
14. Jones, N.G.; Dashwood, R.J.; Jackson, M.; Dye, D. Beta phase decomposition in Ti-5Al-5Mo-5V-3Cr. *Acta Mater.* **2009**, *57*, 3830–3839. [CrossRef]
15. Lutjering, G.; Williams, J.C. *Titanium*; Springer: Berlin, Germany, 2007; pp. 30–33.
16. Nag, S.; Banerjee, R.; Srinivasan, R.; Hwang, J.Y.; Harper, M.; Fraser, H.L. Omega-Assisted nucleation and growth of alpha precipitates in the Ti-5Al-5Mo-5V-3Cr-0.5Fe beta titanium alloy. *Acta Mater.* **2009**, *57*, 2136–2147. [CrossRef]
17. Williams, J.C.; Jaffee, R.I.; Burte, H.M. *Ti1973 Science and Technology*; Plenum Press: New York, NY, USA, 1973; pp. 1433–1494.
18. Williams, J.C.; Fontaine, D.D.; Paton, N.E. The ω-phase as an example of an unusual shear transformation. *Metall. Transform.* **1973**, *4*, 2701–2708. [CrossRef]
19. Blackburn, M.J.T.; Williams, J.C. *Phase Transformation in Ti-Mo and Ti-V Alloys*; Boeing Scientific Research Labs: Seattle, WA, USA, 1968.
20. Zheng, Y.; Williams, R.E.; Sosa, J.M.; Alam, T.; Wang, Y.; Banerjee, R.; Fraser, H.L. The indirect influence of the omega phase on the degree of refinement of distributions of the alpha phase in metastable beta-Titanium alloys. *Acta Mater.* **2016**, *103*, 850–858. [CrossRef]
21. Zheng, Y.F.; Choudhuri, D.; Alam, T.; Williams, R.E.; Benerjee, R.; Fraser, H.L. The role of cuboidal omega precipitates on alpha precipitation in a Ti-20V alloy. *Scr. Mater.* **2016**, *123*, 81. [CrossRef]
22. Li, T.; Kent, D.; Sha, G.; Cairney, J.M.; Dargusch, M.S. The role of ω in the precipitation of α in near-β Ti alloys. *Scr. Mater.* **2016**, *117*, 92–95. [CrossRef]
23. Li, T.; Kent, D.; Sha, G.; Stephenson, L.T.; Ceguerra, A.V.; Ringer, S.P.; Dargusch, M.S.; Cairney, J.M. New insights into the phase transformations to isothermal ω and ω-assisted α in near β-Ti alloys. *Acta Mater.* **2016**, *106*, 353–366. [CrossRef]
24. Azimzaden, S.; Rack, H. Phase transformations in Ti-6.8Mo-4.5Fe-1.5Al. *Met. Mater. Trans. A* **1998**, *29*, 2455–2467. [CrossRef]
25. Shi, R.; Zheng, Y.; Banerjee, R.; Fraser, H.L.; Wang, Y. ω-Assisted α nucleation in a metastable β titanium alloy. *Scr. Mater.* **2019**, *171*, 62–66. [CrossRef]
26. Cao, S.; Jiang, Y.; Yang, R.; Hu, Q.M. Properties of β/ω phase interfaces in Ti and their implications on mechanical properties and ω morphology. *Comput. Mater. Sci.* **2019**, *158*, 49–57. [CrossRef]
27. Sass, S.L. The structure and decomposition of Zr and Ti b.c.c. solid solutions. *J. Less Common. Met.* **1972**, *28*, 157–173. [CrossRef]
28. Ivasishin, P.E.; Markovsky, S.L.; Semiatin, C.H. Ward, Aging response of coarse and fine-grained β titanium alloys. *Mater. Sci. Eng. A* **2005**, *405*, 296–305. [CrossRef]

29. Prima, F.; Vermaut, P.; Texier, G.; Ansel, D.; Gloriant, T. Evidence of α-nanophase heterogeneous nucleation from ω particles in a β-metastable Ti-based alloy by high-resolution electron microscopy. *Scr. Mater.* **2006**, *54*, 645–648. [CrossRef]

30. Mantri, S.A.; Choudhuri, D.; Behera, A.; Hendrickson, M.; Alam, T.; Banerjee, R. Role of isothermal omega phase precipitation on the mechanical behavior of a Ti-Mo-Al-Nb alloy. *Mater. Sci. Eng. A* **2019**, *767*, 138397. [CrossRef]

31. Xu, Y.F.; Yi, D.Q.; Liu, H.Q.; Wang, B.; Yang, F.L. Age-hardening behavior, microstructural evolution and grain growth kinetics of isothermal ω phase of Ti–Nb–Ta–Zr–Fe alloy for biomedical applications. *Mater. Sci. Eng. A* **2011**, *529*, 326–334. [CrossRef]

32. Ke, Y.; He, C.; Zheng, H.; Geng, Y.; Fu, J.; Zhang, S.; Hu, H.; Wang, S.; Zhou, B.; Wang, F.; et al. The time-of-flight Small-Angle Neutron Spectrometer at China Spallation Neutron Source. *Neutron News* **2018**, *29*, 14–17. [CrossRef]

33. Coakley, J.; Vorontsov, V.A.; Jones, N.G.; Radecka, A.; Bagot, P.A.; Littrell, K.C.; Heenan, R.K.; Hu, F.; Magyar, A.P.; Bell, D.C.; et al. Precipitation processes in the Beta-Titanium alloy Ti-5Al-5Mo-5V-3Cr. *J. Alloys Compd.* **2015**, *646*, 946–953. [CrossRef]

34. Sikka, S.K.; Vohra, Y.K.; Chidambaram, R. Omega phase in materials. *Prog. Mater. Sci.* **1982**, *27*, 245–310. [CrossRef]

35. Fontaine, D.D.; Paton, N.E.; Williams, J.C. The omega phase transformation in titanium alloys as an example of displace controlled reactions transformation. *Acta Matallurgica* **1971**, *19*, 1153–1162. [CrossRef]

36. Devaraj, A.; Nag, S.; Srinivasan, R.; Williams, R.E.A.; Banerjee, S.; Banerjee, R.; Fraser, H.L. Experimental evidence of concurrent compositional and structure instabilities leading to ω precipitation in titanium-molybdenum alloys. *Acta Mater.* **2012**, *60*, 596–609. [CrossRef]

37. Sanchez, J.M.; Fontaine, D.D. Anomalous diffusion in omega forming systems. *Acta Matallurgica* **1978**, *26*, 1083–1095. [CrossRef]

38. Furuhara, T.; Maki, T.; Makino, T. Microstructure control by thermomechanical processing in β-Ti-15-3 alloy. *J. Mater. Process. Technol.* **2001**, *117*, 318–323. [CrossRef]

39. Dong, R.; Li, J.; Kou, H.; Fan, J.; Zhao, Y.; Hou, H.; Wu, L. ω-Assisted refinement of α phase and its effect on the tensile properties of a near β titanium alloy. *J. Mater. Sci. Technol.* **2020**, *44*, 24–30. [CrossRef]

40. Alina, G.; Butler, P.; Cho, J.; Doucet, M.; Kienzle, P. SANS Analysis Software. Available online: www.sasview.org (accessed on 12 December 2020).

41. Feigin, L.A.; Svergun, D.I. *Structure Analysis by Small-Angle X-ray and Neutron Scattering*; Plenum Press: New York, NY, USA, 1987.

42. Shi, R.; Ma, N.; Wang, Y. Predicting equilibrium shape of precipitates as function of coherency state. *Acta Mater.* **2012**, *60*, 4172–4184. [CrossRef]

43. Ohmori, Y.; Ogo, T.; Nakai, K.; Kobayashi, S. Effect of ω-phase precipitation on β→α, α″ transformations in a metastable βtitanium alloy. *Mater. Sci. Eng. A* **2001**, *312*, 182–188. [CrossRef]